Smart Structures and Systems, *Vol. 18, No. 5 (2016) 1005-1028*
DOI: http://dx.doi.org/10.12989/sss.2016.18.5.1005

Semi-active control of smart building-MR damper systems using novel TSK-Inv and max-min algorithms

Mohsen Askari*[1], Jianchun Li[2] and Bijan Samali[1]

[1]*Institute for Infrastructure Engineering, University of Western Sydney (UWS), Australia*
[2]*Faculty of Engineering and IT, University of Technology Sydney (UTS), Australia*

(Received August 6, 2015, Revised June 14, 2016, Accepted August 27, 2016)

Abstract. Two novel semi-active control methods for a seismically excited nonlinear benchmark building equipped with magnetorheological dampers are presented and evaluated in this paper. While a primary controller is designed to estimate the optimal control force of a magnetorheological (MR) damper, the required voltage input for the damper to produce such desired control force is achieved using two different methods. The first technique uses an optimal compact Takagi-Sugeno-Kang (TSK) fuzzy inverse model of MR damper to predict the required voltage to actuate the MR dampers (TSKFInv). The other voltage regulator introduced here works based on the maximum and minimum capacities of MR damper at each time-step (MaxMin). Both semi-active algorithms developed here, use acceleration feedback only. The results demonstrate that both TSKFInv and MaxMin algorithms are quite effective in seismic response reduction for wide range of motions from moderate to severe seismic events, compared with the passive systems and performs better than original and Modified clipped optimal controller systems, known as COC and MCOC.

Keywords: semi-active control; MR damper; inverse model; max-min control; TSK fuzzy

1. Introduction

One of the challenging tasks for civil engineers is to mitigate the response of a structure subjected to dynamic loads in order to reduce the risks of damage and injuries caused by extreme hazards such as earthquakes and strong winds. Earthquake engineers, however, have a number of options to design buildings that can resist earthquake loading, e.g. structural elements can be stiffened, bracing can be introduced, the structure can be isolated from the ground (base isolation) or dampers can be used (Li, Yi *et al*. 2011, Yi, Li *et al.* 2013)

Semi-active control uses the measured structural response to determine the required control force. Therefore, they have the ability to deal with the changes in external loading conditions. Furthermore, they cannot input any energy into the system and have properties that can be adjusted in real time and can only absorb or dissipate energy. Because of these properties, there is no stability problem associated with this system (Yang 2001). Another advantage of this system is that, they have an extremely low power requirement which is particularly critical during seismic events

*Corresponding author, Dr., E-mail: m.askari@uws.edu.au

http://www.techno-press.org/?journal=sss&subpage=8 ISSN: 1738-1584 (Print), 1738-1991 (Online)

when the main power source to the structure may fail. These systems also offer the reliability of a passive system, yet maintain the versatility and adaptability of fully active systems. Moreover, they are fail-safe systems as can act as passive control system in the case of power failure (Li, Yi *et al*. 2014).

A magneto-rheological (MR) damper is a type of controllable fluid damper which uses MR fluid. MR fluid has the properties to change reversibly from a free flowing, linear viscous fluid to a semi-solid with controllable yield strength. Because of this property, MR dampers are quite promising for civil engineering applications (Huang, Liu *et al*. 2015). However, the semi active control of MR damper-systems is still a challenging issue in the research community (Esteki, Bagchi *et al*. 2015). A vibration control system using an MR damper requires two main controllers: (i) a primary system controller, and (ii) an MR damper voltage regulator. The former controller computes the desired damping force required for given system conditions. This is typically done through a sliding mode control, linear quadratic Gaussian (LQG) algorithm or any other optimal control theory which makes the real system to emulate an idealised reference system. The function of the voltage regulator is to command the damper to produce the desired force. The effectiveness of this controller depends on its ability to deal with the nonlinear nature of the device (i.e., the nonlinear relationship between damper force and relative velocity across it) and its semi-active nature.

In this paper, two new semi-active control algorithms named TSKInv and MaxMin, are designed to convert the force generated by the primary controller to the required voltage of MR dampers. The first technique uses an optimal compact TSK fuzzy inverse model of MR damper to predict the required voltage to actuate the MR dampers (TSKFInv). To find the inverse model of MR damper, the method introduced by Askari et.al , is used here (Askari, Li *et al.* 2015). Another semi-active voltage controller is also presented which works based on the maximum and minimum capacities of MR damper at each time-step. Using the response of the structure, the maximum and minimum loads that can be generated by an MR damper at each time-step are obtained by a simple forward model of MR damper. Considering a linear relation between these two operating points, the required voltage to produce a desired force is then estimated. The method is designated as MaxMin Optimal Controller. For both algorithms, the acceleration response of building is only used as the input. However, in case the acceleration measurement is not available at some storeys, a Kalman filter is designed to estimate the required unknown response. For the case study, the proposed control strategies are applied to a 20-storey nonlinear benchmark building subjected to 10 different earthquake signals. The numerical results are compared to clipped optimal control (COC) and modified COC and the results discussed.

It should be emphasized that, the idea of using inverse model of MR damper for vibration control purposes, is not new and has been used by other researchers before. However, both controllers developed in this study, are novel on their own, in terms of:

- Learning techniques introduced to model forward and inverse behaviour of MR dampers; a new optimal and compact Takagi-Sugeno fuzzy model using subtractive clustering and genetic algorithm is proposed for modelling the MR dampers.
- Inputs used for the controllers; the inputs used in modelling the MR dampers are selected from time-history of acceleration responses of structure using genetic algorithm. Also the inputs for the controllers are chosen in a way the force feedback is not needed.
- Application of such semi-active controllers in large nonlinear structures under incomplete measurements; the controllers are designed to be able to work with incomplete response of

structure. For example, not all the acceleration response of all floors is needed. In case a required signal is not available, it will be estimated using a Kalman Filter."

More information on each feature will be discussed in the next sections.

2. 3rd generation 20-storey nonlinear benchmark building

The case study considered here, is a benchmark building of 20 storeys designed for the Los Angeles region as defined by Ohtori in the problem definition (Ohtori, Christenson et al. 2004). Based on the literature review, only few semi-active based controls have been reported to mitigate the seismic responses of this benchmark structure (Askari and Davaie-Markazi 2008, Karamodin, Haji-Kazemi *et al*. 2009, Bitaraf, Ozbulut *et al.* 2010, Askari, Li *et al*. 2011, Ozbulut and Hurlebaus 2012, Bitaraf and Hurlebaus 2013).

During large seismic events, structural members can yield, resulting in nonlinear response behaviour that may be significantly different than a linear approximation. To better represent the nonlinear behaviour, a bilinear hysteresis model is used to model the plastic hinges of the building structural members. The bilinear bending properties are predefined for each structural member. These plastic hinges, which are assumed to occur at the moment resisting column-beam and column-column connections, introduce a material nonlinear behaviour of these structures. For more information on how to model the nonlinear behaviour of structural members please refer to (Ohtori, Christenson *et al*. 2004).

Ten earthquake records are used in the simulation, using the original four earthquake records with different intensities. These records are the El Centro (1940) and Hachniohe (1968) earthquake records with 0.5, 1.0, and 1.5 intensity, and Northridge (1994) and Kobe (1995) earthquake records with 0.5 and 1.0 intensity.

25 MR dampers, each with capacity of 1,000 kN are optimally placed throughout the stories of the 20-storey benchmark building as shown in Fig. 1. This configuration is obtained using genetic algorithm as suggested by (Askari, Li *et al*. 2011). However, it is assumed that all dampers on a single floor experience the same inputs.

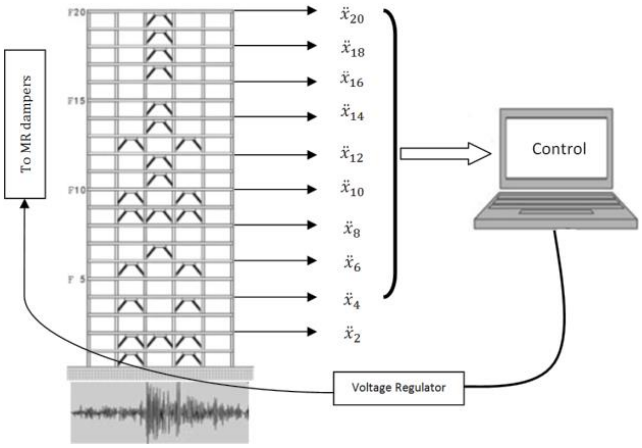

Fig. 1 MR damper and accelerometer configurations

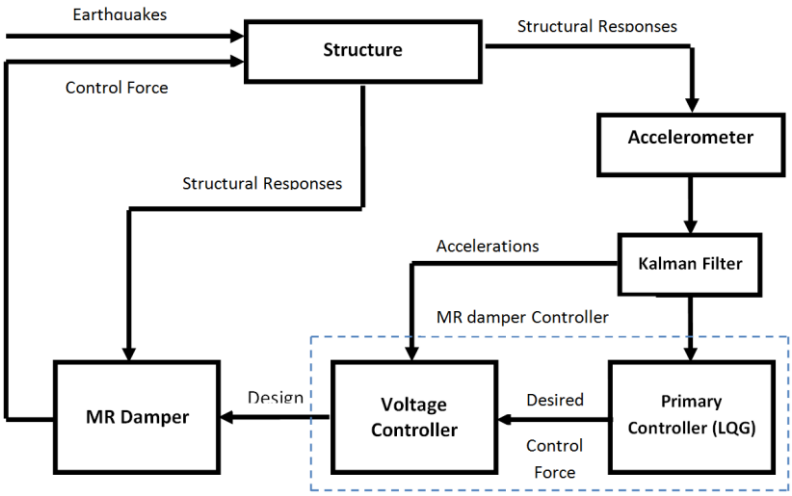

Fig. 2 Block diagram of semi-active control strategy

3. Proposed control strategies

The proposed controller for MR dampers consists of two components which are the primary controller; to produce the desired force and the voltage controller; to convert the desired force to the required voltage of MR dampers (Fig. 2). In this study, a Linear Quadratic Gaussian (LQG) is designed as primary controller. However, there is basically no restriction on the type of primary control algorithm, as the focus of this paper is on the second part, i.e., voltage controller.

Both controllers proposed here, use the acceleration feedback only as accelerometers are more convenient than LVDTs and GPS measurement tools, in terms of installation and cost. Therefore, ten sensors for acceleration measurements are used for feedback into the control system on the 2^{nd}, 4^{th}, 6^{th}, 8^{th}, 10^{th}, 12^{th}, 14^{th}, 16^{th}, 18^{th} and 20^{th} floors. The required accelerations of other storeys are estimated using a Kalman filter observer. More details on how to design the Kalman filter-based LQG controller is presented in appendix.

3.1 Voltage controller 1: Optimal TSK fuzzy inverse controller (TSKFInv)

In this section, a voltage controller based on inverse model of MR damper is proposed. The controller is used to calculate voltage signals to be sent to the MR damper so that it can produce desired optimal control forces estimated by LQG control algorithm.

To design the inverse model of MR damper, it is important to know that, the model should be both accurate and concise to generate a quick and reliable response in real-time applications. In conventional EA-based fuzzy modelling methods, the structure of the FS, e.g., the suitable inputs, are prescribed and then the other parameters of the fuzzy model such as rules and MFs are optimised. However, in many cases the process for selection of inputs and the rule bases for nonlinear systems are co-dependent and therefore these two steps should be done simultaneously especially when enough knowledge on the effect of each input on the performance of the mechanical system does not exist. To solve this problem, some GA based methodologies are then

introduced by researchers. However, all these methods still deals with a large number of to-be-tuned parameters, causing a huge computational burden and hence making the optimisation process very time consuming. Furthermore, application of such method requires a good knowledge of the expected bounds of every parameter at the outset of the design, which may not be available. On the other hand, the excessive number of inputs and rules, not only affect the compactness and transparency of the underlying model, but also increases the complexity of the computations necessary for real-time implementation of the resulting model.

In order to develop an accurate, yet compact FS, in this paper, the algorithm introduced by Askari is employed here to select a small structure fuzzy inference system with acceptable accuracy (Askari, Li *et al.* 2015). In this approach, subtractive clustering is used for initial estimation of the number of clusters as well as the centres. However, in order to find the efficient clusters for each dimension, m, in the input space, the only variable parameter that must be chosen appropriately is the neighbourhood radius r_a. Furthermore, to design an accurate yet compact model, a minimal number of inputs which are the most relevant ones to the model should be selected carefully. To this end, non-dominated sorting genetic algorithm (NSGAII) is hired to intelligently select the required inputs as well as the initial clusters to be modified by fuzzy c-mean (FCM) in the next step.

Since the inverse model uses the delayed force feedback of MR damper, a forward model can be considered to provide the force input and to prevent using load cells. However, if force sensors are not an issue, the sensors' signal is preferable to use. A schematic of TSKFInv controller is shown in Fig. 3. To build such forward model, any parametric or non-parametric model of MR damper can be used. In this study, in order to provide a quick, yet accurate response, a TSK fuzzy model is trained using a set of numerical data. The proposed learning algorithm is as follows:

Step 1: Encode all the parameters into one chromosome using the proposed encoding scheme.

Step 2: Generate the initial population of the chromosomes.

Step 3: Find the initial clusters from the collected data using subtractive clustering method and based on the selected inputs and their corresponding neighbourhood radius values of each chromosome.

Step 4: Update the clusters using FCM using the number and centre of clusters achieved in step 3 for each chromosome.

Step 5: Derive a TSK fuzzy model out of each chromosome, using the proposed obtained clusters and least squares estimator.

Step 6: Based on the resulting rules, fuzzy input structure and the MF parameters, for every chromosome, evaluate three objective functions, namely, the number of inputs, the number of rules and the modelling RMSE. In fact, considering the first two factors as objective functions leads us to have a concise model while the last objective function is the representative of accuracy and can be measured from the following equation, where L is the length of data points, $\hat{Y}$ is the predicted output ("voltage" and "force" in inverse and forward models of MR damper) and Y is the target output

$$J_{RMSE} = \sqrt{\frac{1}{L}\sum_{i=1}^{n}\left(Y_i - \hat{Y}_i\right)^2} \tag{1}$$

Step 7: Rank all the chromosomes based on the objective function values.

Step 8: Choose parents using tournament selection method, to be used in the next step for crossover and mutation.

Step 9: Perform crossover and mutation operators to the parents to generate new set of

individuals called off-springs.

Step 10: Evaluate the objective function of the new individuals and rank them. Steps 3-8 will be repeated for a fixed number of generations. The final answer is the chromosome whose objective function is smaller in the last generation.

3.1.1 Forward model of 1,000 kN MR damper using acceleration feedback only

The forward model describes the force characteristics of the MR damper which depends on the excitation signals when a constant voltage is applied. It can be constructed from many different models, such as modified Bouc–Wen, hyperbolic tangent or phenomenological model.

This research employs the optimal TSK fuzzy model proposed by Askari *et al*., to derive a concise and precise forward model of a 1,000kN MR damper while the voltage is maintained at a maximum level of 10 V (Askari 2015). The output of the forward model is then used as an input signal to the inverse model (Fig. 3).

The dataset used for training process must include all possible ranges of excitation that may be applied to the MR damper during actual operation. The data required for training the proposed fuzzy forward model of MR damper is obtained numerically using the model proposed by (Spencer Jr. *et al.* 1996) and shown in Fig. 4 (Details on physical and mathematical model of Spencer can be found in Appendix). While "T" indicates current time step, the candidate inputs are set to be time histories of acceleration, i.e., $\ddot{x}(T-11), \ddot{x}(T-10), \ldots, \ddot{x}(T)$ as well as voltage, $v(T)$ signals. A time step of 0.01 sec is used to generate 10,000 data points.

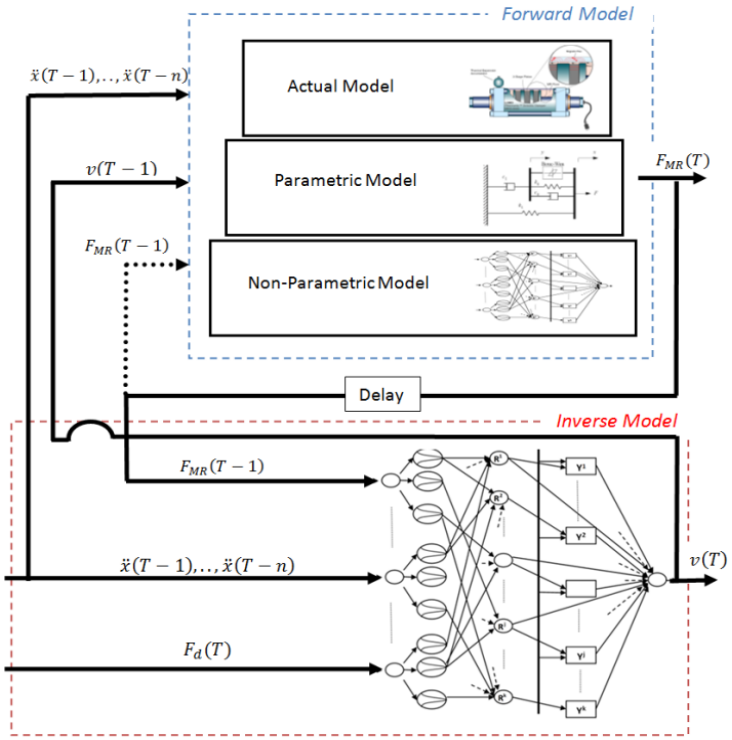

Fig. 3 TSK Fuzzy inverse optimal controller

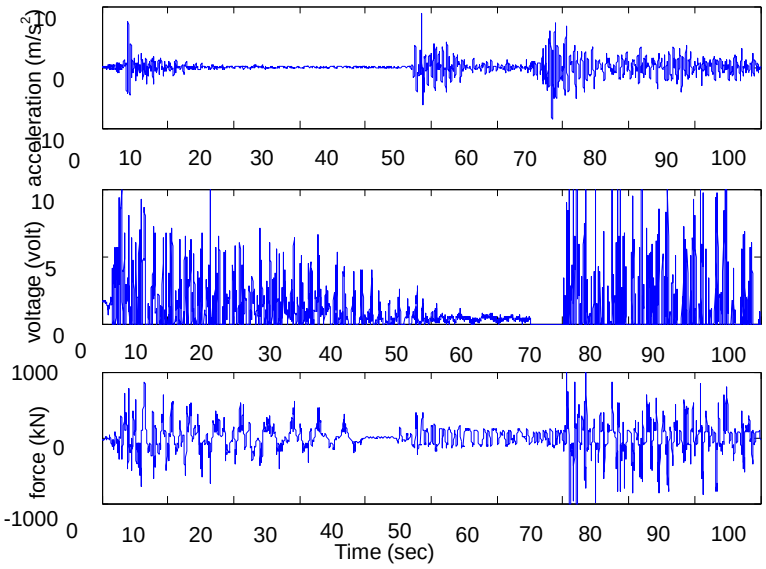

Fig. 4 Collected Training Data

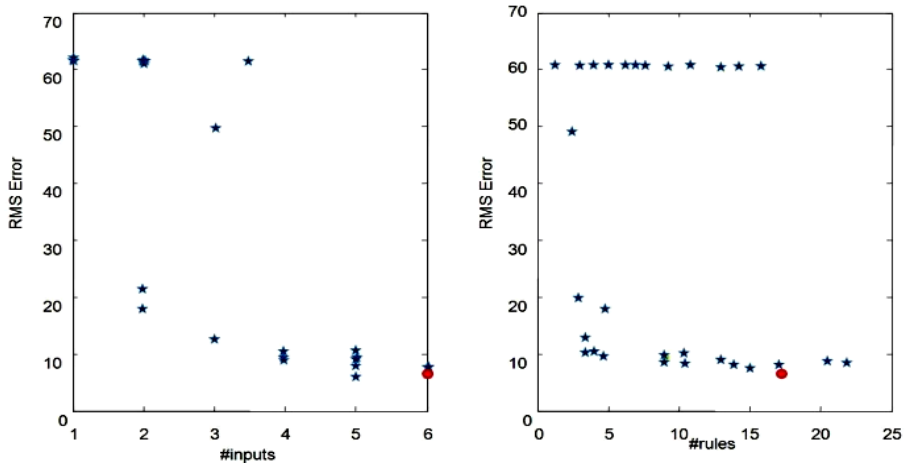

Fig. 5 Pareto front of forward model of MR damper

A Pareto front is then obtained which helps to design a compact and accurate forward model of the MR damper (Fig. 5). Here, the designing point marked by red circle, is selected to build the proposed forward model which uses $\ddot{x}(T-9)$, $\ddot{x}(T-8)$, $\ddot{x}(T-4)$, $\ddot{x}(T-2)$, $\ddot{x}(T)$, $v(T)$ as 6 inputs and has 18 fuzzy rules with RMS error of 8.35. The first 6,500 data-points are chosen for training while the last 3,500 are considered as testing data.

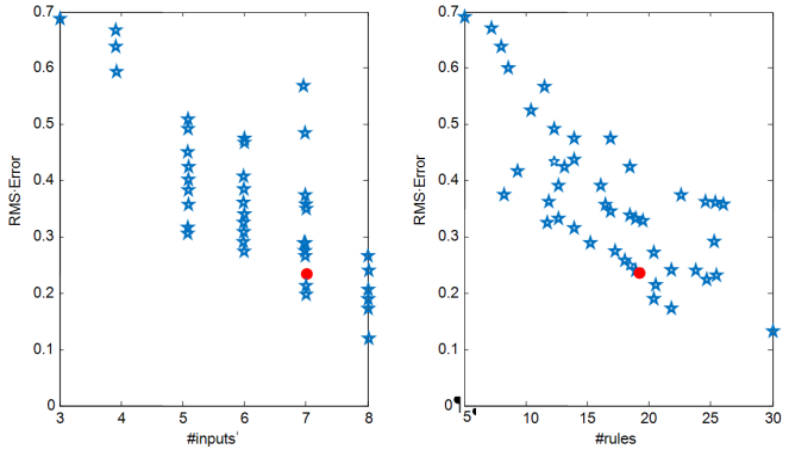

Fig. 6 Pareto front of inverse model of MR damper

3.1.2 Inverse model of 1,000 kN MR damper model

The training process for designing the inverse model of MR damper is to capture the relationship between the applied voltage and the generated force. The training dataset to do so is the same as the dataset used in the previous section and has a 60 s time-span. The inputs of model will be optimally chosen from 16 candidates. The input candidates for the inverse model are floor accelerations; $\ddot{x}(T-14), \ddot{x}(T-13), \ldots, \ddot{x}(T)$, desired force; $F_d(T)$ and also the damper's force; $F_{MR}(T-1)$. The Pareto front achieved after running the optimisation program is shown in Fig. 6. It should be mentioned that, the Pareto front gives freedom to the designer to select the best design based on his desire. If compactness is of more importance to designer, other points can be selected which return more compact models with higher errors. Here the selected point is marked by a red star. The proposed designing point features an inverse fuzzy model with 7 inputs; $\ddot{x}(T-9)$, $\ddot{x}(T-6)$, $\ddot{x}(T-5)$, $\ddot{x}(T-4)$, $\ddot{x}(T-2)$, $F_d(T)$ and $F_{MR}(T-1)$, 19 rules and RMS error of 0.23.

3.2 Voltage controller 2: Max-min optimal controller

Although inverse model of MR damper could estimate the voltage of MR damper to generate a specific desired force, the method needs force feedback which might not be available. Moreover, developing an inverse model is hard due to highly nonlinear behaviour of MR damper. Forward behaviour of MR dampers, on the other hand, is easy to model. Many parametric models are suggested by researchers that can estimate the generated force of the MR damper in different states. Furthermore, they do not necessarily need force feedback to operate.

Here, a new semi-active control algorithm is proposed based on maximum and minimum capacities of the MR damper at each time-step. Depends on the motion of the piston inside MR damper during earthquake, and consequently, the status of MR fluid, damper can generate load in a particular range at each time-step, t, i.e., $[f_{min,t}, f_{max,t}]$. These forces can be found using a simple forward model without using force feedback. Now the control law will be defined as follow

$$v_t = \begin{cases} v_{max} & if \quad |f_{d,t}| > |f_{max,t}| \\ v_{max}\left(\frac{|f_{d,t}|-|f_{min,t}|}{|f_{max,t}|-|f_{min,t}|}\right) & if \quad |f_{min,t}| < |f_{d,t}| < |f_{max,t}| \\ 0 & if \quad |f_{d,t}| < |f_{min,t}| \end{cases} \tag{2}$$

In Eq. (2), $f_{max,t}$ and $f_{min,t}$ are the maximum and minimum generated forces by the MR damper at time t which correspond to passive-on and passive-off forces. $f_{d,t}$ is also the desired force produced by nominal controller (LQG in this study) at time t. So, if the desired force is less than minimum capacity of the MR damper at time t, the voltage will be set to 0. Similarly, if the desired force is larger than maximum capacity of the MR damper; $f_{max,t}$, the voltage to be sent to the MR damper will be maximum; v_{max}, to produce a force to be as close as possible to the desired force. But, if the desired force is between the maximum and minimum forces of the MR damper, then the voltage takes a portion of maximum voltage. This portion is found by interpolation using a linear relationship between max/min voltage and max/min force of the MR damper. It is interesting to note that if we assume, $f_{min,t}$ and $f_{max,t}$ to be equal to 0 and the total capacity of the MR damper (which is 1,000kN in this study) respectively, then the proposed algorithm is similar to Modified Clipped Optimal Controller. However, this assumption is not correct as the maximum and minimum of the MR damper's forces at each time-step are functions of structural responses which are again functions of time. A schematic diagram for the controller is shown in Fig. 8. To find $f_{min,t}$ and $f_{max,t}$, one of the parametric forward models can be used. However, the complex ones, such as modified Bouc-Wen, are not very applicable to large real-time problems since they are time consuming and the simple ones, on the other hand, are not accurate enough. Therefore, the TSK fuzzy forward model, developed in previous section, will be used to provide the maximum and minimum of damper force at each time-step using acceleration feedback.

4. Numerical results

Two proposed semi-active strategies are validated through a highly nonlinear 20-storey benchmark building under 10 different ground accelerations. To make a comparison, an active control system, semi-active COC and Modified COC systems, together with two passive systems, passive off (POFF) and passive on (PON) are also designed. A *Simulink* model in MATLAB was used to implement the six different control strategies. For the passive control models the voltage is constant, whereas for the semi-active control models, the voltage is obtained through the respective control algorithms.

The comparison between the desired force developed by LQG and the MR damper's generated force using COC, MCOC, TSKFInv and MaxMin algorithms on the 20th floor, are depicted in Fig. 9 to Fig. 12 for 4 different earthquakes, each with intensity of 1. Also the required voltages of the MR damper to generate such forces, using the aforementioned semi-active control approaches, are compared with each other in the same figures. For the sake of better observation and understanding, this comparison is done for a short period of time. The force time history shown in these figures, illustrates the improvement introduced by MaxMin and TSKFInv algorithms compared to original COC and MCOC. The differences in MR damping forces are attributable to

the voltage commanded by the different algorithms. For the MCOC, the voltage varies continuously between zero and a portion of maximum voltage ($v = \mu v_{max}$). This is in stark contrast to the original COC, for which the control voltage can only take two values, 0 and v_{max}.

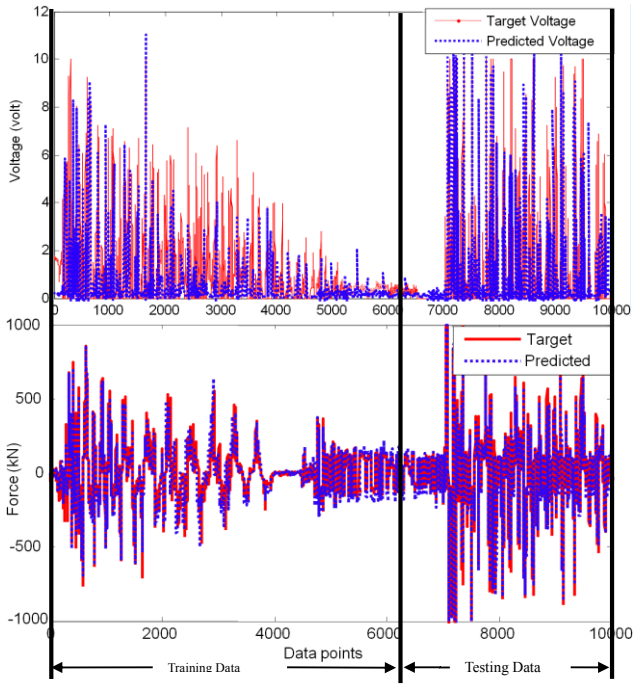

Fig. 7 Comparison between target and predicted voltage and target and predicted force (bottom) using fuzzy inverse and forward models of MR damper

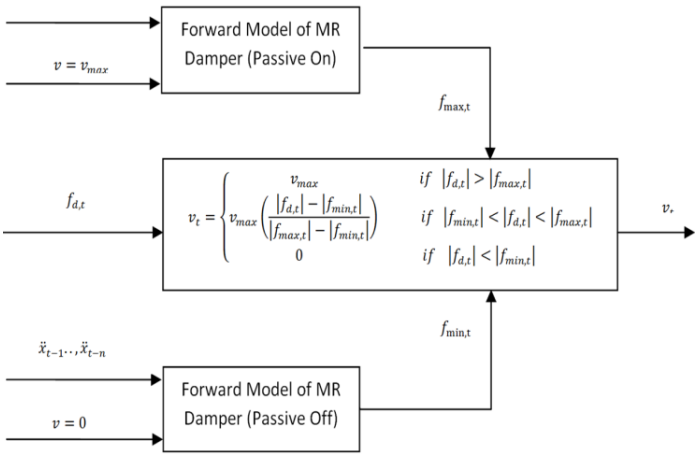

Fig. 8 Schematic diagram of MaxMin optimal controller (proposed in this study)

Unlike these two algorithms, both inverse and MaxMin models try to estimate the exact value of voltage which results in generating smooth and robust force signals being very close to the desired force. Consequently, the error between target and MR damper's forces generated by MaxMin and TSKFInv models are less than the original and modified versions of COC. These two methods can also successfully track the desired force while the generated force of COC and MCOC, in comparison, fluctuate a lot and produce many overshoots. As a consequence, the average force and voltage of COC is more than the other semi-active control algorithms. On the other hand, it can be seen that the absolute generated force of the MR damper using MCOC is, most of the time, smaller than the absolute force generated by the other three semi-active control strategies. This is because of the intention of MCOC to work with zero voltage in a wide range of situations, in particular when desired force is less than the damper's force while in reality the voltage is not zero as can be seen from the graphs of voltage history.

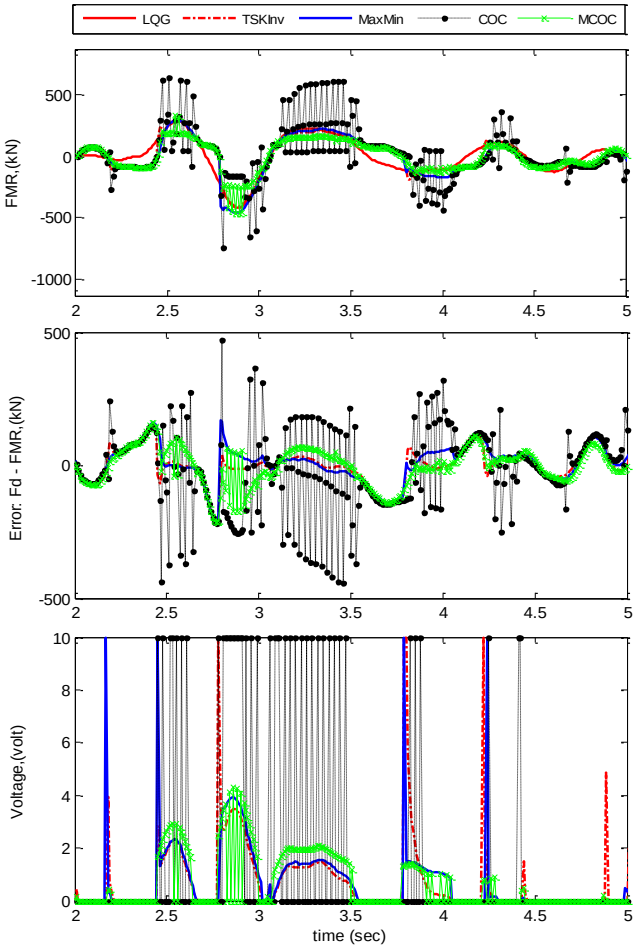

Fig. 9 MR damper's force and voltage at 20th floor (El-Centro, intensity: 1.0)

The force time history shown in these figures, illustrates the improvement introduced by MaxMin and TSKFInv algorithms compared to original COC and MCOC. The differences in MR damping forces are attributable to the voltage commanded by the different algorithms. For the MCOC, the voltage varies continuously between zero and a portion of maximum voltage ($v = \mu v_{max}$). This is in stark contrast to the original COC, for which the control voltage can only take two values, 0 and v_{max}. Unlike these two algorithms, both inverse and MaxMin models try to estimate the exact value of voltage which results in generating smooth and robust force signals being very close to the desired force. Consequently, the error between target and MR damper's forces generated by MaxMin and TSKFInv models are less than the original and modified versions of COC. These two methods can also successfully track the desired force while the generated force of COC and MCOC, in comparison, fluctuate a lot and produce many overshoots. As a consequence, the average force and voltage of COC is more than the other semi-active control algorithms. On the other hand, it can be seen that the absolute generated force of the MR damper using MCOC is, most of the time, smaller than the absolute force generated by the other three semi-active control strategies. This is because of the intention of MCOC to work with zero voltage in a wide range of situations, in particular when desired force is less than the damper's force while in reality the voltage is not zero as can be seen from the graphs of voltage history.

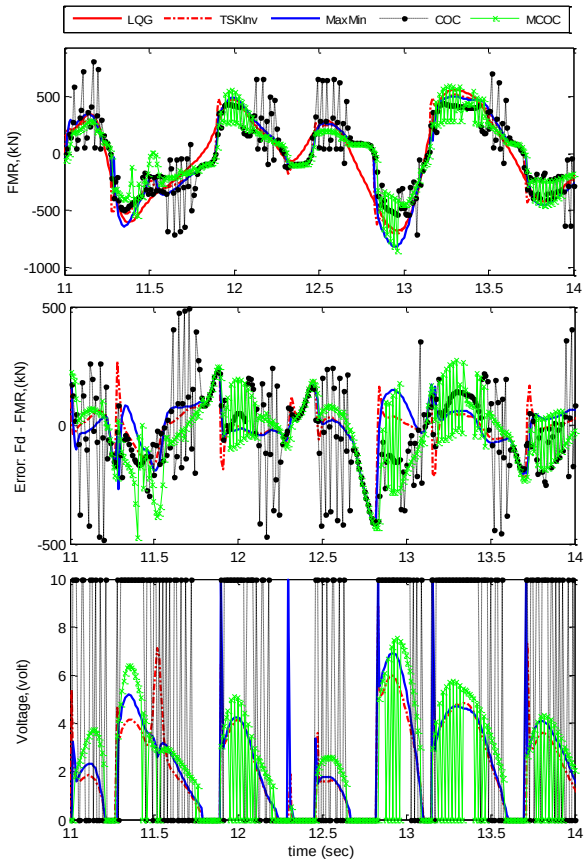

Fig. 10 MR damper's force and voltage at 20th floor (Kobe, intensity:1.0)

The comparison between performances of the two newly proposed semi-active control algorithms also shows that, although both are very effective in tracking the desired force signal, TSKFInv model performs slightly better as it is able to capture almost the exact inverse dynamics of the MR damper and, thus, command the MR damper better than MaxMin which uses a linear relationship between voltage and force of damper.

To systematically evaluate the control performance of each controller, fourteen of evaluation indices defined in the benchmark problem statement (Table 1) are determined and presented in Table and Table . Also, to understand the effectiveness of each control algorithm, the performance of each algorithm are compared with those of the active (Ac), original and modified clipped optimal control algorithms (COC, MCOC), passive-on (v=10) and passive-off (v=0) (Table and 3). However, it is noted that the original and modified clipped-optimal and TSKInv (without combining with forward model) controllers require the use of force feedback through either sensor measurements or a non-parametric forward model to achieve this level of performance.

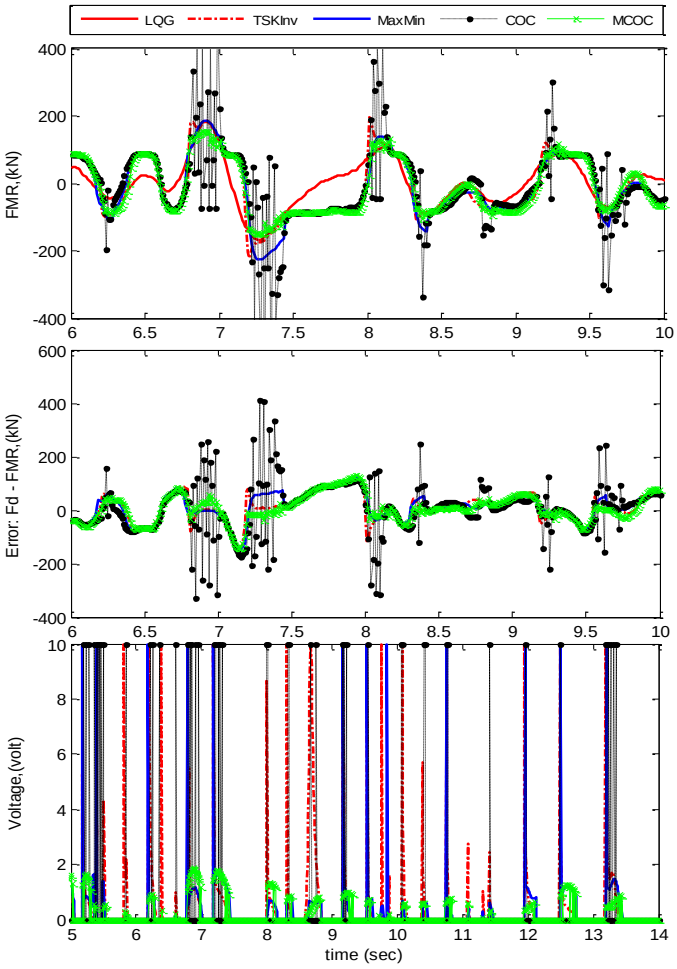

Fig. 11 MR damper's force and voltage at 20th floor (Hachinohe, intensity:1.0)

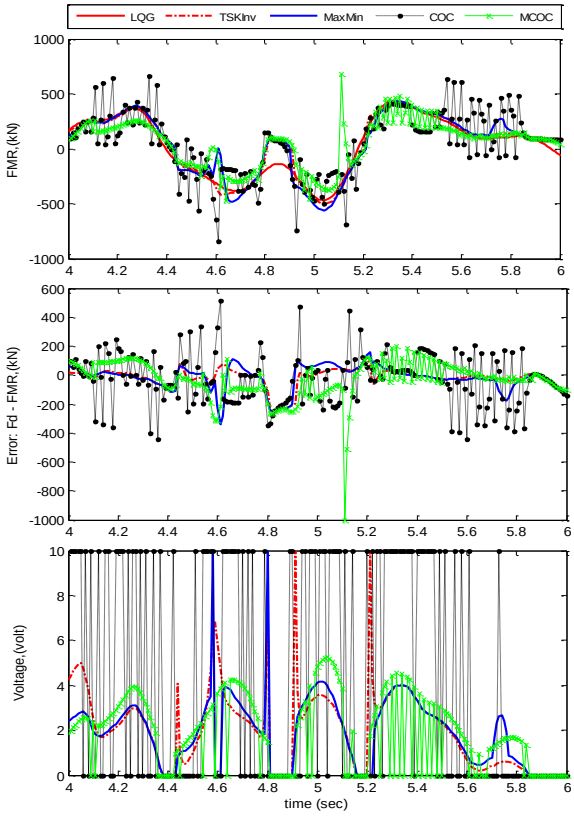

Fig. 12 MR damper's force and voltage at 20th floor (Northridge, intensity:1.0)

Table 1 Structural evaluation indices (Ohtori, Christenson *et al*. 2004)

J_1	Inter-storey Drift Ratio	J_8	Dissipated Energy
J_2	Level Acceleration	J_9	Plastic Connections
J_3	Base Shear Force	J_{10}	Normed Ductility
J_4	Normed Inter-storey Drift Ratio	J_{11}	Control Force
J_5	Normed Level Acceleration	J_{12}	Control Device Stroke
J_6	Normed Base Shear	J_{13}	Control Power
J_7	Ductility	J_{14}	Normed Control Power

The idea of developing a voltage controller is to make the MR damper generate the closest force to the desired one produced by nominal controller (LQG in this study). In other words, an ideal semi-active voltage controller is the one that can track the performance of the designed active controller. From Tables 2 and 3, it is seen that compared with COC and MCOC, active controller, in most cases, performs better in terms of reduction of objective indices.

Table 2 Structural evaluation criteria (J_1 to J_7)

Controller		El-Centro			Hachinohe			Northridge		Kobe		Max
		0.5	1.0	1.5	0.5	1.0	1.5	0.5	1.0	0.5	1.0	
J_1	Active	0.742	0.743	0.742	0.867	0.871	0.887	0.840	0.947	0.784	0.678	0.947
	COC	0.751	0.717	0.720	0.870	0.862	0.897	0.824	0.916	0.705	0.835	0.916
	MCOC	0.764	0.752	0.744	0.899	0.898	0.916	0.867	0.914	0.790	0.923	0.923
	TSKFIN	0.756	0.731	0.735	0.880	0.874	0.899	0.844	0.914	0.736	0.730	0.914
	MaxMin	0.759	0.741	0.736	0.902	0.893	0.910	0.847	0.913	0.748	0.654	0.913
	P-ON	0.602	0.598	0.606	0.609	0.629	0.705	0.659	0.845	0.378	0.580	0.845
	P-OFF	0.772	0.811	0.989	0.909	0.921	0.957	0.921	0.937	0.909	0.896	0.957
J_2	Ac	0.639	0.635	0.652	0.710	0.705	0.796	0.777	0.844	0.665	0.842	0.844
	COC	0.800	0.820	0.750	0.932	0.849	0.898	0.869	0.977	0.722	0.938	0.977
	MCOC	0.693	0.692	0.720	0.913	0.845	0.924	0.931	0.923	0.718	0.886	0.931
	TSKFIN	0.626	0.613	0.624	0.841	0.756	0.836	0.906	0.835	0.668	0.828	0.906
	MaxMin	0.666	0.646	0.655	0.923	0.828	0.883	0.912	0.874	0.677	0.931	0.931
	P-ON	3.628	1.811	1.238	5.271	2.635	2.044	1.605	1.137	1.289	0.970	5.271
	P-OFF	0.790	0.839	1.055	0.943	0.955	1.061	1.015	1.144	0.848	1.004	1.144
J_3	Ac	0.760	0.763	0.888	0.973	0.977	0.995	0.885	0.983	0.921	1.024	1.024
	COC	0.767	0.840	0.924	1.015	0.984	1.013	0.877	0.993	0.938	1.040	1.040
	MCOC	0.772	0.784	0.908	0.995	0.981	1.009	0.880	0.985	0.981	1.072	1.072
	TSKFIN	0.767	0.786	0.914	0.995	0.981	1.008	0.880	0.985	0.962	1.039	1.039
	MaxMin	0.776	0.778	0.902	0.995	0.981	1.008	0.880	0.988	0.965	1.047	1.047
	P-ON	0.980	0.859	0.943	1.093	1.000	1.031	0.925	1.085	0.594	1.177	1.177
	P-OFF	0.772	0.812	0.948	0.996	0.982	1.008	0.930	0.986	1.017	1.034	1.034
J_4	Ac	0.681	0.680	0.686	0.885	0.884	0.905	0.768	0.998	0.672	0.225	0.998
	COC	0.589	0.605	0.624	0.836	0.844	0.865	0.651	0.923	0.544	0.276	0.923
	MCOC	0.613	0.638	0.663	0.840	0.848	0.871	0.695	0.933	0.629	0.278	0.933
	TSKFIN	0.605	0.625	0.644	0.838	0.846	0.869	0.670	0.951	0.571	0.200	0.951
	MaxMin	0.605	0.630	0.653	0.838	0.847	0.870	0.683	0.938	0.582	0.217	0.938
	P-ON	0.456	0.440	0.454	0.687	0.716	0.740	0.387	1.006	0.234	0.123	1.006
	P-OFF	0.621	0.659	0.700	0.840	0.852	0.881	0.811	0.869	0.706	0.588	0.881
J_5	Ac	0.556	0.554	0.572	0.648	0.644	0.654	0.614	0.646	0.586	0.713	0.713
	COC	0.513	0.497	0.520	0.626	0.613	0.621	0.546	0.615	0.531	0.694	0.694
	MCOC	0.573	0.572	0.595	0.661	0.666	0.678	0.615	0.662	0.613	0.764	0.764
	TSKFIN	0.548	0.538	0.554	0.644	0.641	0.650	0.574	0.626	0.564	0.698	0.698
	MaxMin	0.547	0.549	0.567	0.648	0.650	0.658	0.589	0.636	0.578	0.714	0.714
	P-ON	16.482	7.707	4.994	21.885	10.469	6.799	7.946	6.159	8.563	6.365	21.885
	P-OFF	0.597	0.627	0.688	0.672	0.708	0.742	0.712	0.767	0.732	0.885	0.885
J_6	Ac	0.746	0.745	0.751	0.855	0.855	0.865	0.825	0.867	0.729	0.881	0.881
	COC	0.666	0.676	0.693	0.820	0.816	0.828	0.702	0.816	0.635	0.803	0.828
	MCOC	0.687	0.705	0.728	0.830	0.831	0.844	0.744	0.822	0.679	0.843	0.844
	TSKFIN	0.679	0.693	0.711	0.825	0.823	0.836	0.720	0.818	0.653	0.815	0.836
	MaxMin	0.677	0.697	0.718	0.826	0.827	0.840	0.734	0.823	0.666	0.820	0.840
	P-ON	0.685	0.605	0.581	0.950	0.873	0.826	0.441	0.705	0.352	0.590	0.950
	P-OFF	0.694	0.725	0.764	0.833	0.843	0.862	0.783	0.845	0.748	0.892	0.892
J_7	Ac	0.776	0.776	0.724	0.958	0.962	0.942	0.742	0.980	0.729	0.698	0.980
	COC	0.732	0.742	0.686	0.944	0.949	0.916	0.680	0.946	0.677	0.711	0.949
	MCOC	0.757	0.768	0.735	0.952	0.955	0.928	0.731	0.945	0.782	0.802	0.955
	TSKFIN	0.747	0.752	0.708	0.949	0.952	0.925	0.693	0.947	0.716	0.697	0.952
	MaxMin	0.748	0.760	0.717	0.947	0.951	0.922	0.706	0.946	0.728	0.690	0.951
	P-ON	0.659	0.652	0.597	0.677	0.730	0.690	0.596	0.846	0.297	0.533	0.846
	P-OFF	0.768	0.808	0.833	0.953	0.956	0.929	0.839	0.945	0.929	0.764	0.956

Table 3 Structural evaluation criteria (J_8 to J_{14})

J_8	Ac	0.000	0.000	0.047	0.000	0.000	0.639	0.267	0.572	0.222	0.307	0.639
	COC	0.000	0.000	0.002	0.000	0.000	0.600	0.092	0.508	0.172	0.321	0.600
	MCOC	0.000	0.000	0.063	0.000	0.000	0.661	0.157	0.572	0.332	0.565	0.661
	TSKFIN	0.000	0.000	0.018	0.000	0.000	0.633	0.109	0.509	0.235	0.233	0.633
	MaxMin	0.000	0.000	0.033	0.000	0.000	0.633	0.127	0.517	0.260	0.238	0.633
	P-ON	0.000	0.000	0.000	0.000	0.000	0.002	0.000	0.310	0.000	0.048	0.310
	P-OFF	0.000	0.000	0.325	0.000	0.000	0.697	0.332	0.853	0.604	0.751	0.853
J_9	Ac	0.000	0.000	0.465	0.000	0.000	0.698	0.542	0.906	0.308	0.833	0.906
	COC	0.000	0.000	0.209	0.000	0.000	0.581	0.333	0.906	0.308	0.857	0.906
	MCOC	0.000	0.000	0.581	0.000	0.000	0.721	0.563	0.917	0.333	0.940	0.940
	TSKFIN	0.000	0.000	0.419	0.000	0.000	0.628	0.354	0.896	0.308	0.845	0.896
	MaxMin	0.000	0.000	0.419	0.000	0.000	0.698	0.396	0.896	0.308	0.857	0.896
	P-ON	0.000	0.000	0.000	0.000	0.000	0.000	0.000	0.823	0.000	0.536	0.823
	P-OFF	0.000	0.000	0.860	0.000	0.000	0.814	0.875	1.000	0.667	1.000	1.000
J_{10}	Ac	0.764	0.763	0.682	0.860	0.860	0.932	0.663	1.014	0.841	0.238	1.014
	COC	0.645	0.669	0.614	0.814	0.818	0.891	0.549	0.927	0.562	0.238	0.927
	MCOC	0.664	0.698	0.645	0.822	0.829	0.896	0.615	0.952	0.831	0.492	0.952
	TSKFIN	0.658	0.687	0.630	0.818	0.824	0.902	0.576	0.958	0.723	0.207	0.958
	MaxMin	0.658	0.692	0.638	0.819	0.826	0.898	0.591	0.944	0.744	0.250	0.944
	P-ON	0.449	0.455	0.422	0.651	0.699	0.715	0.294	1.013	0.211	0.139	1.013
	P-OFF	0.671	0.717	0.689	0.824	0.841	0.861	0.779	0.901	0.762	0.723	0.901
J_{11}	Ac	0.00204	0.00405	0.00605	0.00173	0.00322	0.00458	0.00642	0.00770	0.00584	0.00920	0.00920
	COC	0.00557	0.00682	0.00760	0.00518	0.00666	0.00738	0.00803	0.00807	0.00718	0.00920	0.00920
	MCOC	0.00159	0.00468	0.00725	0.00144	0.00363	0.00507	0.00667	0.00856	0.00666	0.00920	0.00920
	TSKFIN	0.00251	0.00449	0.00700	0.00219	0.00351	0.00494	0.00677	0.00911	0.00623	0.00920	0.00920
	MaxMin	0.00271	0.00401	0.00601	0.00170	0.00321	0.00454	0.00605	0.00795	0.00578	0.00920	0.00920
	P-ON	0.00816	0.00898	0.00920	0.00799	0.00886	0.00920	0.00920	0.00920	0.00920	0.00920	0.00920
	P-OFF	0.00088	0.00101	0.00920	0.00084	0.00092	0.00098	0.00109	0.00920	0.00107	0.00920	0.00920
J_{12}	Ac	0.074	0.074	0.074	0.076	0.07	0.081	0.079	0.102	0.131	0.106	0.131
	COC	0.073	0.073	0.073	0.074	0.075	0.080	0.074	0.099	0.127	0.131	0.131
	MCOC	0.073	0.076	0.076	0.073	0.074	0.080	0.078	0.099	0.139	0.145	0.145
	TSKFIN	0.073	0.074	0.075	0.073	0.074	0.080	0.075	0.099	0.133	0.115	0.133
	MaxMin	0.073	0.075	0.075	0.073	0.074	0.080	0.076	0.099	0.134	0.104	0.134
	P-ON	0.056	0.055	0.059	0.045	0.055	0.065	0.064	0.089	0.052	0.096	0.096
	P-OFF	0.073	0.078	0.092	0.073	0.074	0.079	0.086	0.099	0.156	0.141	0.156
J_{13}	Ac	0.00129	0.00254	0.00400	0.00058	0.00117	0.00174	0.00308	0.00502	0.00363	0.00797	0.00797
	COC	0.00223	0.00320	0.00410	0.00149	0.00295	0.00411	0.00354	0.00480	0.00480	0.00855	0.00855
	MCOC	0.00137	0.00292	0.00439	0.00088	0.00121	0.00166	0.00295	0.00486	0.00326	0.00746	0.00746
	TSKFIN	0.00170	0.00281	0.00436	0.00107	0.00170	0.00232	0.00335	0.00568	0.00362	0.00845	0.00845
	MaxMin	0.00143	0.00257	0.00396	0.00096	0.00138	0.00198	0.00293	0.00511	0.00340	0.00779	0.00779
	P-ON	0.00908	0.00775	0.00904	0.00879	0.00737	0.00883	0.00635	0.00933	0.00931	0.01543	0.01543
	P-OFF	0.00113	0.00141	0.00616	0.00081	0.00093	0.00100	0.00103	0.00480	0.00159	0.00773	0.00773
J_{14}	Ac	0.00005	0.00009	0.00015	0.00003	0.00006	0.00010	0.00007	0.00011	0.00007	0.00013	0.00015
	COC	0.00008	0.00014	0.00020	0.00007	0.00011	0.00016	0.00009	0.00013	0.00008	0.00015	0.00020
	MCOC	0.00007	0.00011	0.00016	0.00006	0.00009	0.00012	0.00008	0.00011	0.00007	0.00013	0.00013
	TSKFIN	0.00007	0.00012	0.00018	0.00006	0.00010	0.00014	0.00008	0.00013	0.00008	0.00015	0.00015
	MaxMin	0.00007	0.00012	0.00017	0.00006	0.00009	0.00013	0.00008	0.00012	0.00008	0.00014	0.00014
	P-ON	0.00347	0.00177	0.00125	0.00135	0.00183	0.00148	0.00105	0.00101	0.00127	0.00105	0.00347
	P-OFF	0.00007	0.00011	0.00014	0.00006	0.00009	0.00011	0.00006	0.00008	0.00006	0.00009	0.00011

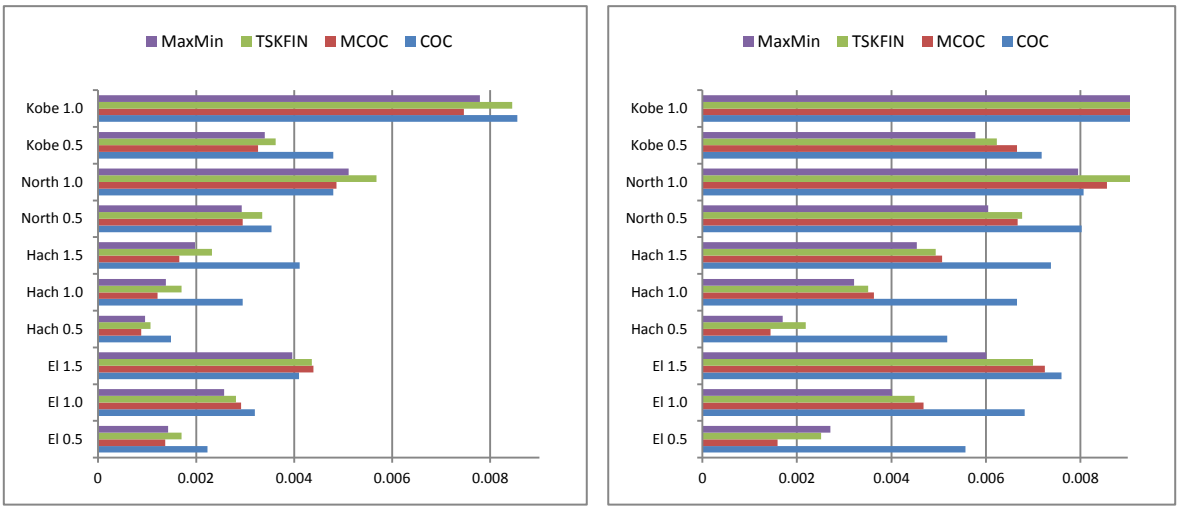

Fig. 13 Structural control force and power comparison between different semi-active control algorithms

For these cases, J values of TSKFInv and Max-Min algorithms are either better than active controller or between active controller and COC. On the other hand, in some cases such as drift related indices, i.e., J_1 and J_4, COC and MCOC suppress the norm acceleration more than active system and, therefore, the objective values of TSKFInv and Max-Min algorithms, which are better controllers in tracking the desired force, are closer to active one and, therefore, more than COC and MCOC.

Results also show that both new proposed semi-active algorithms have very similar performances, although TSKInv is slightly better. In particular, these two algorithms are able to reduce the peak drift ratio and peak floor acceleration for all ten earthquakes by up to 35% and 38%, respectively, noting that a reduction in acceleration response of individual floors can be directly related to forces and, hence, to the mass and amount of material needed in each floor to resist the earthquake loads. This is while COC can only reduce the peak floor acceleration by 25%. The other performance indices which are important to reduce are the control force and power. Due to the fact that COC algorithm operates by switching the voltage of the MR dampers between two extremes, i.e., passive-on (v=10) and passive-off (v=0), it works with the maximum load on many occasions unnecessarily and often causes force overshoots as shown in Fig. 9 to Fig. 12. As a consequence, the maximum control force and power indices, i.e. J_{11} and J_{13} of COC are more than the other semi-active control algorithms considered in this study. MCOC, in contrast, has the least control power consumption as it works with zero or a small portion of voltage during the earthquake. However, at some point, due to inaccurate dynamic mapping of the MR damper, it also produces unnecessary forces, even though compared to COC, these forces are much less. MaxMin and TSKInv on the other hand, make a trade-off between reduction of structural responses, control force and power consumption. Graphical comparisons of control force and power indices between the four aforementioned semi-active algorithms are shown in Fig. 13. It shows that, in terms of peak control force reduction (J_{11}), MaxMin, TSKInv, MCOC and COC

have the best performances while the least control power consumption belongs to MCOC, MaxMin, TSKInv and COC, respectively.

The last column of Table 2 indicates the maximum values of objective indices of the structure under 10 earthquake signals (the maximum of each row). This is called the worst case scenario as defined in the benchmark problem. The first six performance criteria of these objective indices are compared with each other for different control algorithms in Fig. 14. It can be observed that both TSKFInv and MaxMin algorithms are able to track the performance of active controller closely which proves their superiority over COC and MCOC. Moreover, as can be seen, passive-on algorithm is the best in suppression of the peak drift ratio while it is the worse one in reduction of peak values of the acceleration, peak and normalised base shear, peak and normalised level acceleration and normalised drift ratio. The reason is due to working with maximum load and hence exerting too much resisting force which causes an overshoot in the response of structure.

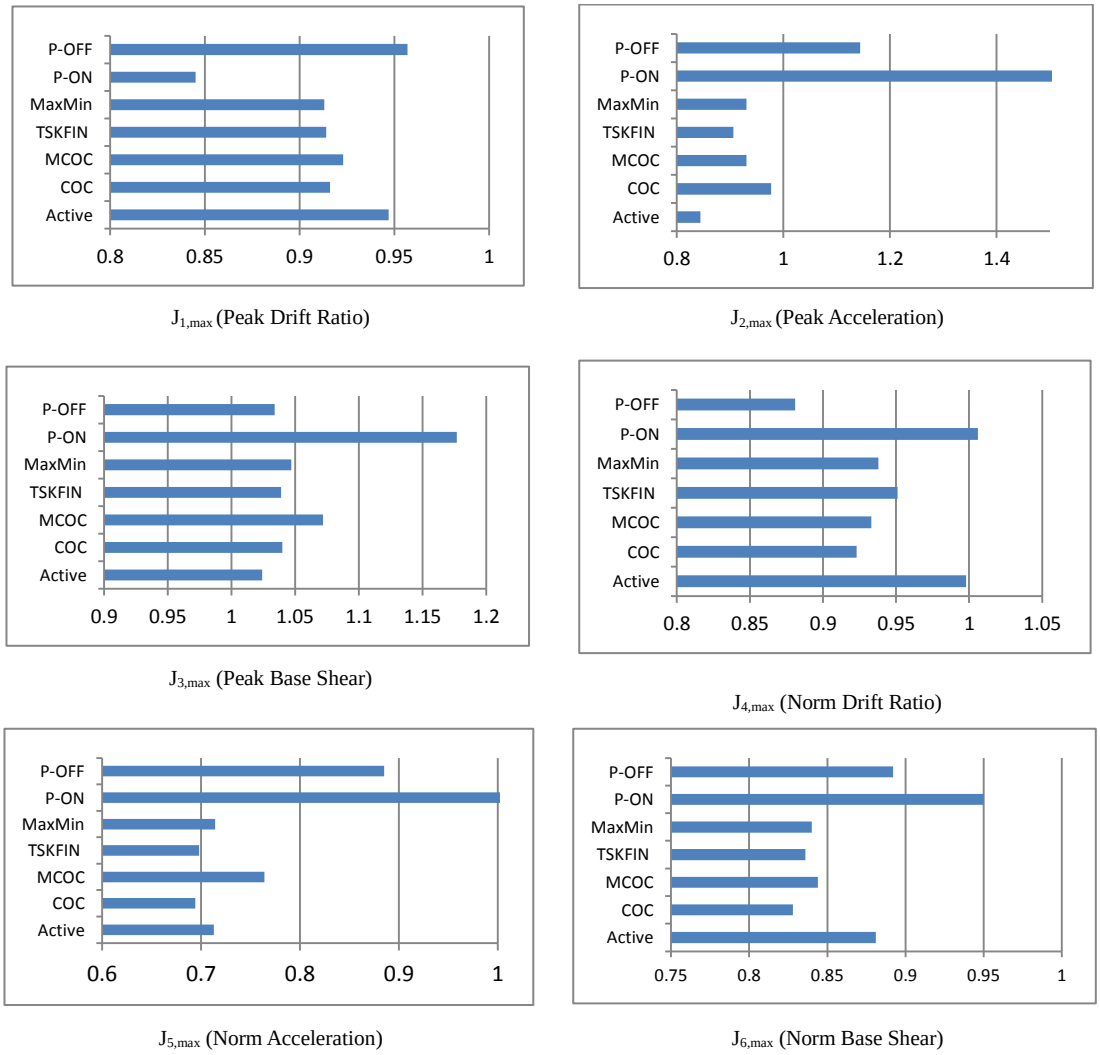

$J_{1,max}$ (Peak Drift Ratio)

$J_{2,max}$ (Peak Acceleration)

$J_{3,max}$ (Peak Base Shear)

$J_{4,max}$ (Norm Drift Ratio)

$J_{5,max}$ (Norm Acceleration)

$J_{6,max}$ (Norm Base Shear)

Fig. 14 Performance criteria (worst-case scenario)

Table 4 Computational effort comparison between different control algorithms for 20 seconds of El-Centro earthquake with intensity of 1

	Active (LQG)	**COC**	**MCOC**	**TSKInv**	**MaxMin**
Running Time	16.8 s	207.1	208.4 s	227.8 s	235.1 s
Force Feedback	-	Yes	Yes	Yes	No
Structural response feedback	Acc	-	-	Acc	Acc (+velocity)

In order to compare the computational effort of the algorithms under study, the simulation running time of each semi-active algorithm for 20 seconds of El-Centro earthquake with intensity of 1 is presented in Table 4. The MATLAB codes were ran on an "Intel Pentium, Core 2Duo, CPU E8500, 3.16 GHz, 3.25 GB of RAM" with time step of 0.01s as defined in the benchmark problem. The other features of four aforementioned algorithms are also compared with each other in the same table. The numerical model of the MR damper used in the *SIMULINK* is the modified Bouc-Wen model which is highly nonlinear and computationally expensive. Therefore, the running time of the semi-active controllers, which use MR dampers, are numerically large where COC and MCOC provide the quickest response as they work with simple control laws and MaxMin method has the largest running time since it uses two fuzzy models to estimate the maximum and minimum capacities of the MR damper. In this study, a forward model of the MR damper is trained, using acceleration feedback to provide the required force feedback to TSKInv model. However, depending on the complexity of the model and availability of force sensors, one can directly use the actual force measurements. Moreover, instead of using the acceleration response of the structure to build and train the forward and inverse models of MR damper, other states of the structure can be employed.

The top floor absolute acceleration and the inter-storey drift between the 19th and 20th floors of uncontrolled, TSKFInv and MaxMin controlled, in time domain, are shown in Fig. 15 for El-centro, Kobe, Hachinohe and Northridge earthquakes with intensity of 0.5. For the other floors and earthquakes, similar observations can be made. Maximum acceleration and inter-storey drift ratio response profiles are also provided for all floors of the building. According to these time history results, the peak relative acceleration and inter-storey drift are reduced using both semi-active control algorithms. The response profiles show the reduction in peak drift ratio as well as acceleration in almost all floors. Moreover, the figures show that both newly developed voltage regulating algorithms perform very similar to each other. However, MaxMin method performs slightly better.

5. Conclusions

In this paper, new technologies for improving structural resistance to earthquake loading were investigated. Two new semi-active control algorithms, named TSKInv and MaxMin, were devised to convert the force generated by the nominal controller (LQG here) to the required voltage for MR dampers.

TSKInv algorithm was developed by modelling the inverse dynamics of MR damper using TSK fuzzy inference systems. The structure of model was optimised to select the best minimal inputs and fuzzy rules which lead to an accurate model. To provide the force feedback to the

inverse model, another fuzzy model was trained to capture the forward dynamics of the MR damper. The second algorithm was designed based on the maximum ($v = v_{max}$) and minimum ($v = v_{min}$) load of the MR damper at each time-step. Then, assuming a linear relationship between damper's voltage and force, a decision is made for voltage regulation in order to generate a specific desired force. Both methods use only the acceleration feedback.

The models were critically evaluated against passive damping as well as the original and modified clipped optimal controller through a highly nonlinear 20-storey benchmark building. Evaluation was further conducted on the basis of performance criteria to show the effectiveness on reduction of quake-induced vibrations of the building structure via a set of ratios (indices) for the controlled and uncontrolled cases, respectively.

Results illustrate that the proposed new control algorithms can effectively track the desired control force and perform much better than COC and MCOC in terms of structural response reduction using less control force and power. Also, the comparison between MaxMin and TSKInv shows that MaxMin model uses less control power while TSKInv decreases the structural response more. However, MaxMin is easier to use, although computationally is slightly more expensive than TSKFInv. Ability to operate without force measurement is the other benefit of MaxMin model.

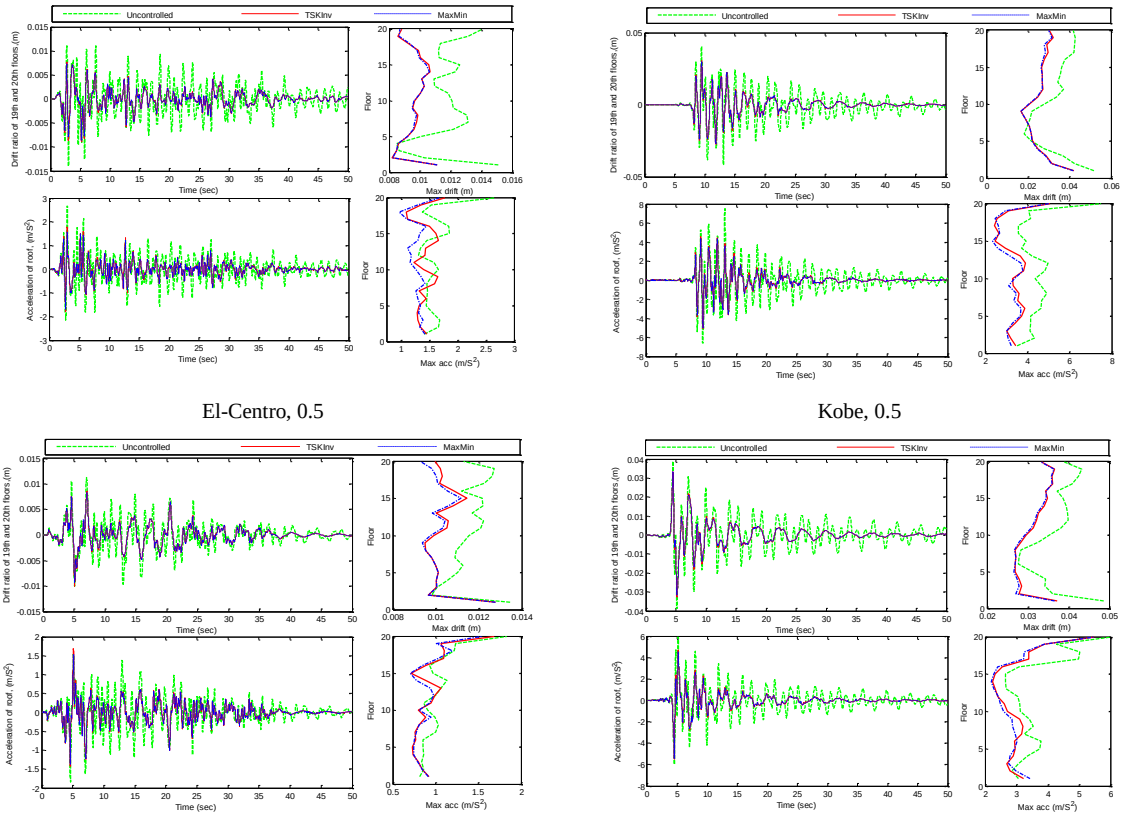

El-Centro, 0.5 Kobe, 0.5

Hachinohe, 0.5 Northridge, 0.5

Fig. 15 Structural Response

References

Askari, M. and Davaie-Markazi, A.H. (2008), "Multi-objective optimal fuzzy logic controller for nonlinear building-MR damper system", *Proceedings of the Systems, Signals and Devices, 2008. IEEE SSD 2008. 5th International Multi-Conference on, IEEE*.

Askari, M., Li, J. and Samali, B. (2011), "Semi-active LQG control of seismically excited nonlinear buildings using optimal Takagi-Sugeno inverse model of MR dampers", *Procedia Eng*., **14**, 2765-2772.

Askari, M., Li, J., Samali, B. and Gu, X. (2015), "Experimental forward and inverse modelling of magnetorheological dampers using an optimal Takagi–Sugeno–Kang fuzzy scheme", *J. Intel. Mat. Syst. Str*., 1045389X15604403.

Bitaraf, M. and Hurlebaus, S. (2013), "Semi-active adaptive control of seismically excited 20-story nonlinear building", *Eng. Struct*., **56**, 2107-2118.

Bitaraf, M., Ozbulut, O.E., Hurlebaus, S. and Barroso, L. (2010), "Application of semi-active control strategies for seismic protection of buildings with MR dampers", *Eng. Struct*., **32**(10), 3040-3047.

Esteki, K., Bagchi, A. and Sedaghti, R. (2015), "Semi-active control of seismic response of a building using MR fluid-based tuned mass damper", *Smart Struct. Syst*., **16**(5), 807-833.

Huang, H., Liu, J. and Sun, L. (2015), "Full-scale experimental verification on the vibration control of stay cable using optimally tuned MR damper", *Smart Struct. Syst*., **16**(6), 1003-1021.

Karamodin, A., Haji-Kazemi, H., Rowhanimanesh, A. and Akbarzadeh Totonchi, M.R. (2009), "Semi-active control of structures using a neuro-inverse model of MR dampers", *Scientia Iranica*, **16**, 256-263.

Li, H.N., Yi, T.-H., Jing, Q.Y., Huo, L.S. and Wang, G.X. (2011), "Wind-induced vibration control of Dalian international trade mansion by tuned liquid dampers", *Math. Probl. Eng*., **2012**.

Li, H.N., Yi, T.H., Ren, L., Li, D.S. and Huo, L.S. (2014), "Reviews on innovations and applications in structural health monitoring for infrastructures", *Struct. Monit. Maint*., **1**(1), 1-45.

Ohtori, Y., Christenson, R., Spencer Jr., B.F. and Dyke, S. (2004), "Benchmark control problems for seismically excited nonlinear buildings", *J. Eng. Mech. - ASCE*, **130**(4), 366-385.

Ozbulut, O.E. and Hurlebaus, S. (2012), "Application of an SMA-based hybrid control device to 20-story nonlinear benchmark building", *Earthq. Eng. Struct. D*., **41**(13), 1831-1843.

Spencer Jr., B.F., Dyke, S., Sain, M. and Carlson, J. (1997), "Phenomenological model for magnetorheological dampers", *J. Eng. Mech. - ASCE*, **123**(3), 230-238.

Yang, G. (2001), Large-scale magnetorheological fluid damper for vibration mitigation: modeling, testing and control, University of Notre Dame.

Yi, T.H., Li, H.N. and Sun, H.M. (2013), "Multi-stage structural damage diagnosis method based on", *Smart Struct. Syst*., **12**(3-4), 345-361.

Ze-bing, D., Jin-zhi, H. and Hong-xia, W. (2004), "Semi-active control of a cable-stayed bridge under multiple-support excitations", *J. Zhejiang University Sci*., **5**(3), 317-325.

CY

Appendix

1.1 Phenomenological model of MR damper

The modified Bouc-Wen model of MR damper, referred to phenomenological model, is shown in Fig. 16 and expressed by the the following differential equations (Spencer, Dyke *et al.* 1997)

$$F = c_1\dot{y} + k_1(x - x_0)$$
$$\dot{y} = \frac{1}{c_0 + c_1}[\alpha z + c_0\dot{x} + k_0(x - y)]$$
$$\dot{z} = -\gamma|\dot{x} - \dot{y}|z|z|^{n-1} - \beta(\dot{x} - \dot{y})|z|^n + A(\dot{x} - \dot{y})$$
$$\alpha = \alpha_a + \alpha_b u$$
$$c_1 = c_{1_a} + c_{1_b} u$$
$$c_0 = c_{1_a} + c_{1_b} u$$
$$\dot{u} = -\eta(u - v),$$

where z and α , called evolutionary variables, describe the hysteretic behaviour of the MR damper; c_0 and c_1 are viscous damping at high and low velocities, respectively; k_0 and k_1 are the stiffness at large velocities and the accumulator stiffness, respectively; the x_0 is the initial displacement of spring with stiffness k_1; γ, β and A are adjustable shape parameters of the hysteresis loops; and v and u are input and output voltages of a first-order filter, respectively.
A set of typical parameters of the 1000kN MR damper is presented in Table 5 (Ze-bing, Jin-zhi *et al.* 2004).

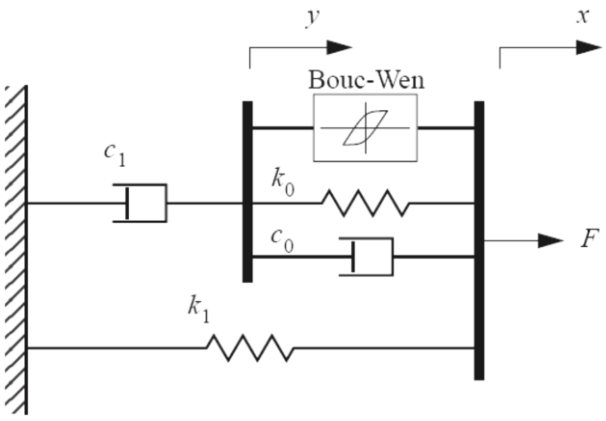

Fig. 16 Modified Bouc-Wen model of the MR Damper (Spencer, Dyke *et al*. 1997)

Table 5 Typical Parameters of a 1000kN MR Damper

Parameter	Values	Parameter	Values	Parameter	Values
$\mathbf{c_{0_a}(kNs/m)}$	110.0	α_a(kN/m)	46.2	k_1 (kN/m)	0.0097
$\mathbf{c_{0_b}(kNs/mV)}$	114.3	α_b(kN/mV)	41.2	x_0 (m)	0.18
$\mathbf{k_0}$ **(kN/m)**	0.002	$\gamma(m^{-2})$	164.0	n	2
$\mathbf{c_{1_a}(kNs/m)}$	8359.2	$\beta(m^{-2})$	164.0	$\eta(s^{-1})$	100
$\mathbf{c_{1_b}(kNs/m)}$	7481.9	A	1107.2		

1.2 Primary controller (LQG) and Kalman Filter observer design

Although there is no limitation on the type of controllers, as long as it measures the desired force based on the system response, a Linear Quadratic Gaussian (LQG) controller is designed in this study using the acceleration feedbacks (measured and estimated), to generate the desired control force to be passed to the inverse model of MR damper.

The force vector for control devices can be modelled as

$$f = K_f u$$

where K_f is a matrix that accounts for multiple actuators per level.

Because the benchmark building model is quite large, a reduced-order model of the system, designated as the design model, is developed for purposes of control design. The equations relevant to this 20-storey structure is given as

$$\dot{x}^d = A_d x^d + B_d u + E_d \ddot{x}_g$$

$$y_{md} = D_s(C_{md} x^d + D_{md} u + F_{md} \ddot{x}_g) + \upsilon$$

$$y_{ed} = C_{ed} x^d + D_{ed} u + F_{ed} \ddot{x}_g$$

where x^d is the design state vector, $y_{md} = [\ddot{x}_{a2}, \ddot{x}_{a4}, \ddot{x}_{a6}, \ddot{x}_{a8}, \ddot{x}_{a10}, \ddot{x}_{a12}, \ddot{x}_{a14}, \ddot{x}_{a16}, \ddot{x}_{a18}, \ddot{x}_{a20}]^T$ is the vector of measured responses , $y_{ed} = [\ddot{X}_{a1} \dots \ddot{X}_{a20}]^T$ is the vector of the regulated responses (lateral acceleration at each floor), u is the control signal for the control force of the individual ideal actuators, and A_d, B_d, E_d, C_{md}, D_{md}, F_{md}, C_{ed}, D_{ed}, and F_{ed} are reduced-order coefficient matrices.

To simplify designing of the LQG controller, $\ddot{X}_g$ is taken to be a stationary white noise, and an infinite horizon performance index is chosen that weighs the accelerations of the floors, i.e.,

$$\hat{J} = \lim_{\tau \to \infty} \frac{1}{\tau} E[\int_0^\tau \{(C_{ed} x^d + D_{ed} u)^T Q (C_{ed} x^d + D_{ed} u) + Ru^2\} dt]$$

where R=[16 × 16] matrix with equal weighting placed on each actuator force (i.e., R=(1/16)[I]) and the weighting matrix Q is chosen to be a [16 ×16] matrix with equal weighting placed on each of the level accelerations (i.e., Q=3 × 109[I]). The ground acceleration and measurement noises are assumed to be identically distributed, and the ratio of the power spectral densities is taken to be

$$\frac{S_{\ddot{x}_g \ddot{x}_g}}{S_{v_i v_i}} = \gamma_g = 25.$$

The separation principle allows the control and estimation problems to be considered separately, yielding a control law of the form

$$u = -\underset{\sim}{K}\hat{x}^d$$

where $\hat{x}^d$ is the Kalman filter estimate of the state vector based on the reduced-order design model, including the actuator model. $\underset{\sim}{K}$ is the full state feedback gain matrix for the deterministic regulator problem given by

$$\underset{\sim}{K} = \tilde{R}^{-1}(\tilde{N} + B_d^T \underset{\sim}{P})$$

where $\underset{\sim}{P}$ is the solution of the algebraic Riccati equation given by

$$\underset{\sim}{P}\tilde{A} + \tilde{A}^T \underset{\sim}{P} - \underset{\sim}{P} B_d \tilde{R}^{-1} B_d^T \underset{\sim}{P} + \tilde{Q} = 0$$

and

$$\tilde{Q} = C_{ed}^T Q C_{ed} - \tilde{N}\tilde{R}^{-1}\tilde{N}^T$$

$$\tilde{N} = C_{ed}^T Q D_{ed}$$

$$\tilde{R} = R + D_{ed}^T Q D_{ed}$$

$$\tilde{A} = A_d - B_d \tilde{R}^{-1}\tilde{N}^T$$

Calculations to determine $\underset{\sim}{K}$ were done using the MATLAB routine lqry.m within the control toolbox. The Kalman filter optimal estimator is given by

$$\dot{\hat{x}}^d = A_d \hat{x}^d + B_d u + L(y_s - C_{md}\hat{x}^d - D_{md}u)$$

$$L = [\underset{\sim}{R}^{-1}(\gamma_g F_{md} E_d^T + C_{md} S)]^T$$

Where S is the solution of the algebraic Riccati equation given by

$$S\underset{\sim}{A} + \underset{\sim}{A}^T S - S\underset{\sim}{G}S + \underset{\sim}{H} = 0$$

and

$$\underset{\sim}{A} = A_d^T - C_{md}^T \underset{\sim}{R}^{-1}(\gamma_g F_{md} E_d^T)$$

$$\underset{\sim}{G} = C_{md}^T \underset{\sim}{R}^{-1} C_{md}$$

$$\underset{\sim}{H} = \gamma_g E_d E_d^T - \gamma_g^2 E_d F_{md}^T \underset{\sim}{R}^{-1} F_{md} E_d^T$$

$$\underset{\sim}{R} = I + \gamma_g F_{md} F_{md}^T$$

Calculations to determine L were done using the MATLAB routine lqe.m within the control toolbox.